

Article

Behaviour of Zinc Complexes and Zinc Sulphide Nanoparticles Revealed by Using Screen Printed Electrodes and Spectrometry

Lukas Nejd1^{1,2}, Branislav Ruttkay-Nedecky^{1,2}, Jiří Kudr¹, Monika Kremplova¹,
Natalia Cernei^{1,2}, Jan Prasek², Marie Konecna^{1,2}, Jaromir Hubalek², Ondrej Zitka^{1,2},
Jindrich Kynicky^{3,4}, Pavel Kopel², Rene Kizek² and Vojtech Adam^{1,2,*}

¹ Department of Chemistry and Biochemistry, Faculty of Agronomy, Mendel University in Brno, Zemedelska 1, Brno CZ-613 00, Czech Republic; E-Mails: lukasnejdl@gmail.com (L.N.); brano.ruttkay@seznam.cz (B.-R.N.); george.kudr@centrum.cz (J.K.); monika.kemplova@seznam.cz (M.K.); cernei.natalia3@gmail.com (N.C.); mariekon@centrum.cz (M.K.); zitkao@seznam.cz (O.Z.)

² Central European Institute of Technology, Brno University of Technology, Technicka 3058/10, Brno CZ-616 00, Czech Republic; E-Mails: prasek@feec.vutbr.cz (J.P.); hubalek@feec.vutbr.cz (J.H.); paulko@centrum.cz (P.K.); kizek@sci.muni.cz (R.K.)

³ Department of Geology and Pedology, Faculty of Forestry and Wood Technology, Mendel University in Brno, Zemedelska 1, Brno CZ-613 00, Czech Republic; E-Mail: jindrak@email.cz

⁴ Karel Englis College, Sujanova Square 356/1, Brno CZ-602 00, Czech Republic

* Author to whom correspondence should be addressed; E-Mail: vojtech.adam@mendelu.cz; Tel.: +420-545-133-350; Fax: +420-545-212-044.

Received: 1 August 2013; in revised form: 3 September 2013 / Accepted: 8 October 2013 /

Published: 25 October 2013

Abstract: In this study, we focused on microfluidic electrochemical analysis of zinc complexes ($Zn(phen)(his)Cl_2$, $Zn(his)Cl_2$) and ZnS quantum dots (QDs) using printed electrodes. This method was chosen due to the simple (easy to use) instrumentation and variable setting of flows. Reduction signals of zinc under the strictly defined and controlled conditions (pH, temperature, flow rate, accumulation time and applied potential) were studied. We showed that the increasing concentration of the complexes ($Zn(phen)(his)Cl_2$, $Zn(his)Cl_2$) led to a decrease in the electrochemical signal and a significant shift of the potential to more positive values. The most likely explanation of this result is that zinc is strongly bound in the complex and its distribution on the electrode is very limited. Changing the pH from 3.5 to 5.5 resulted in a significant intensification of the Zn(II)

reduction signal. The complexes were also characterized by UV/VIS spectrophotometry, chromatography, and ESI-QTOF mass spectrometry.

Keywords: electrochemical analysis; differential pulse voltammetry; screen printed electrode; spectrometry; Zn(II)

1. Introduction

Zinc is an essential element playing numerous crucial roles in organisms. It is involved especially in the synthesis of proteins and DNA [1], because zinc stabilizes the structure of chromatin and affects replication of DNA and transcription of RNA by regulating the activity of transcription factors for RNA and DNA polymerases [2]. Zinc is also essential to stabilize the structure of proteins containing zinc finger motifs [3]. Zinc is further closely connected with the production of insulin [4], and in light of this fact, zinc complexes could find an application in the treatment of diabetes [5]. Zn(II) complexes are able to modulate an inflammatory response by influencing the secretion and activity of several inflammation-related cytokines and enzymes [6]. Moreover, xylan-chitooligomer-zinc complex exhibited antioxidant and antimicrobial activity [7]. Transition metal complexes that are capable of cleaving DNA under physiological conditions are of interest in the development of anticancer drugs [8]. Cisplatin and related platinum-based drugs bind covalently to DNA, but they have side effects, especially, toxicity and acquired drug resistance, that requires the development of new drugs, which bind non-covalently to DNA, are less toxic and are target-specific. Among the non-platinum complexes for metal based chemotherapy, copper and zinc complexes have been much explored due to the fact that both copper and zinc are bioessential elements responsible for numerous bioactivities in living organisms [9–11]. Role of zinc and copper complexes as potential chemotherapeutic compounds have been confirmed, both complexes were able to bind and cleave DNA [12]. Zinc sulphide (ZnS) is one of the first semiconductors discovered and it has shown remarkable properties, versatility and a promise for novel diverse applications, including light-emitting diodes (LEDs), electroluminescence, flat panel displays, infrared windows, sensors, lasers, and biodevices, *etc.* [13]. Its atomic structure and chemical properties are comparable to more popular and widely known ZnO [14]. In the past decade, numerous results have been reported on the synthesis of nanometer scale semiconductor crystals (quantum dots, nanowires, nanorods, *etc.*) because their properties, due to quantum confinement effect, dramatically change and, in most cases, improve as compared with their bulk counterparts [15–17]. Among them, ZnS quantum dots (QDs) as semiconductor nanocrystals with a typical size of 2–10 nm have been attracting much interest [18]. An advantage of ZnS QDs is that they can be analysed electrochemically [19].

There is a wide range of well-established techniques for detection of metals, including the most widely used mass spectrometry and atomic absorption spectrometry. These methods are reliable and highly sensitive. On the other hand, they require expensive instrumentation and involve time-consuming procedures. Electrochemical methods represent another class of widely used techniques for the detection of metal ions. Anodic stripping voltammetry has become one of the most important techniques [20–22] in this field, together with hanging mercury drop electrode (HMDE) [23–25]. The

disadvantage of this method is the difficulty of miniaturization, especially due to the hanging drop, which needs the supply of gas. Another disadvantage of the mercury electrode is its limited modification possibilities, a small anodic range (limited by the oxidation of mercury) and the high toxicity of mercury. Mercury electrodes also cannot be used in a flow system.

Despite their sensitivity issues, screen printed electrodes (SPEs) are a suitable alternative to HMDE. The low acquisition costs of lithographic equipment have enabled the widespread use of disposable SPEs as biosensors and chemical sensors in microfluidic systems. Microfluidics is a technology that requires lower volumes of sample, increases the speed of analysis and response time, allowing a massive parallelization for high-throughput analysis, and reducing the cost of fabrication of biosensors [26–28]. In recent years, methods involving the coupling of microfluidics with electrochemical techniques have been increasing because of the benefits associated with miniaturization, automation, sensitivity and specificity [29–35].

Based on the abovementioned facts we investigated the combination of zinc as a central atom, 1,10-phenanthroline (phen) as a versatile N-N chelating aromatic ligand that can interact with DNA by π - π interaction and histidine as an amino acid with a side chain aromatic ring. Aromatic ligands also play an important role in enhancing DNA binding and cleavage activity. We also selected histidine as a ligand because it is known that amino acids/peptides recognize a specific base sequence of DNA and that aromatic ring contributes to the stabilization of proteins through hydrophobic interactions and the formation of hydrophilic environments [36].

2. Experimental Section

2.1. Chemicals and Materials

ZnCl₂, Zn(NO₃)₂·6H₂O, L-histidine, 1,10-phenanthroline, 3-mercaptopropionic acid, and Na₂S·9H₂O, all of ACS purity, were purchased from Sigma-Aldrich (St. Louis, MO, USA). Stock solutions were prepared using ACS water immediately before use. pH values were measured using an inoLab Level 3 instrument (Wissenschaftlich-Technische Werkstätten GmbH; Weilheim, Germany). Deionised water underwent demineralization by reverse osmosis using an Aqua Osmotic 02 system (Aqua Osmotic, Tisnov, Czech Republic) and was subsequently purified using a Millipore RG system MiliQ water, 18 M Ω , (Millipore Corp., Billerica, MA, USA).

2.1.1. Preparation of Zinc Nitrate Hexahydrate

Stock solution of zinc nitrate (1 mM) was prepared by dissolving of zinc nitrate hexahydrate (0.297 g) in water (1 L).

2.1.2. Preparation of Zn(phen)(his)Cl₂

ZnCl₂ (0.136 g) was dissolved in water (10 mL). A suspension of histidine (0.155 g) and 1,10-phenanthroline (0.2 g) in water (90 mL) was added to the ZnCl₂ solution under constant stirring. The reaction mixture was placed in an ultrasonic bath for 30 min and dissolution of reaction components occurred. After that, the reaction mixture was stirred overnight. The resulting colourless solution was used for measurements.

2.1.3. Preparation of Zn(his)Cl₂

Preparation of the complex was the same as for Zn(phen)(his)Cl₂, but only histidine was added to the ZnCl₂ solution. A colourless solution was obtained.

2.1.4. Preparation of ZnS Quantum Dots (QDs)

ZnS MPA (MPA = 3-mercaptopropionic acid) QDs were prepared using the slightly modified method published in [18,19,37]. Zinc nitrate hexahydrate Zn(NO₃)₂·6H₂O (0.03 g, 0.1 mM) was dissolved in ACS water (25 mL). 3-Mercaptopropionic acid (35 µL, 0.4 mM) was added slowly to the stirring solution. Afterwards, the pH was adjusted to 9.1 with 1 M NH₃ (1.5 mL). Sodium sulphide nonahydrate Na₂S·9H₂O (0.024 g, 0.1 mM) in ACS water (22 mL) was poured into the first solution under vigorous stirring. The obtained colourless solution was then stirred for 1 h.

2.2. UV/VIS —Spectrophotometry

Absorption spectra were recorded using a SPECORD 210 spectrophotometer (Analytik Jena, Jena, Germany) in the range 200–400 nm and in steps of 1 nm. Quartz cuvettes with 1 cm optical path (Hellma, Essex, UK) were used. The cell with cuvette was thermostated to 20 °C with a Julabo thermostat (Labortechnik, Wasserburg, Germany). Absorption spectra were recorded after 60 min of interaction and were evaluated using the WinASPECT program, version 2.2.7.0.

Spectral Analysis of Zinc

Zinc forms a red chelate complex with 2-(5-bromo-2-pyridylazo)-5-(N-propyl-N-sulfo-propylamino)phenol (Nitro-PAPS) with an absorption maximum at $\lambda = 560$ nm. The colour intensity is proportional to the total zinc concentration in the sample. A volume of 800 µL of reagent (Greiner, Frickenhausen, Germany), 0.02 mM 2-(5-bromo-2-pyridylazo)-5-(N-propyl-N-sulphopropylamino)phenol, 170 mM sodium citrate, and 4 mM dimethylglyoxime in 200 mM bicarbonate buffer, pH 9.8) was pipetted into plastic cuvette and subsequently 40 µL of the sample was added. Spectra were recorded after 5 min long incubation of a reagent with a sample. After a measurement, cuvettes were rinsed with deionised water and dried with nitrogen.

2.3. Screen Printed Electrodes' System

2.3.1. Electrode System Design

The electrode system was designed and fabricated as a disposable planar three-electrode sensor in the LabSensNano laboratories (Brno University of Technology, Brno, Czech Republic). The 25.4 × 7.2 mm dimensions of the 0.625 mm thick alumina electrode substrate were achieved by a dividing of standard 2 × 2" piece of the substrate. The shape and theoretical working area of electrodes were designed according to the previous optimization process [38]. In accordance with the optimization results, the working electrode (WE) was designed to be as large as possible (in this case geometrically comparable with the diameter of the GCE of 3 mm with a working area of 7.1 mm²), reference electrode (RE) 1.3 mm² and auxiliary electrode (AE) 6.2 mm².

2.3.2. Electrode System Fabrication

The screen-printed sensor was fabricated using a semiautomatic Aurel C880 screen-printer (Aurel Automation, Modigliana, Italy) and fired using a BTU fast fire furnace for the thick-film processing (BTU, North Billerica, MA, USA). The conductive layer was fabricated from AgPdPt-based paste (ESL 9562-G). The protective layer was fabricated from dielectric paste (ESL 4917). AE was fabricated from Pt-based paste (ESL 5545). All cermet pastes were obtained from ESL ElectroScience Europe, Berkshire, UK and fired at 850 °C according to the recommended values in the products datasheets. WE was a screen-printed electrode fabricated using a special carbon paste for electrochemical sensor electrodes (DuPont BQ221, DuPont Company, Wilmington, DE, USA) and cured at 130 °C for 10 min according to the manufacturer's datasheet. RE was screen-printed using a special polymer Ag/AgCl paste (DuPont 5874, Ag:AgCl ratio 65:35) and dried at 120 °C for 5 min.

2.3.3. Microfluidic Analysis with Electrochemical (Differential Pulse Voltammetry) Detection

Printed electrodes (three-electrode system) and a flow cell were used. The flow cell was designed in the shape of a cuboid with sides of 1 cm (width) × 1.5 cm (height) × 3 cm (length). The reaction zone was designed for 10 µL of analyte with 0.7 mm wide inlet and outlet channel. The sample was injected using a peristaltic pump (Amersham Biosciences, Glattbrugg, Sweden). Changes in the reduction signal were recorded with a PGSTAT 101 potentiostat (Metrohm, Herisau, Switzerland) and the results were evaluated by the NOVA 1.8 software (Metrohm). Settings of the potentiostat were as it follows: initial potential −1.7 V, end potential −0.1 V, step potential 0.01 V, modulation amplitude 0.1 V, modulation time 0.004 s, interval time 0.1 s, equilibration time 5–130 s. Samples were diluted with acetate buffer pH 3.3–5.5 and measured at temperature from 10 to 50 °C (both parameters were optimized). Screen-printed sensors and analysis solutions were thermostated (10–50 °C) before measurement by a Julabo thermostat.

2.4. Differential Pulse Voltammetric Determination of Zinc Using HMDE

Determination of zinc by the differential pulse voltammetry was performed with a 663 VA Stand (Metrohm) using a standard cell with three electrodes. A hanging mercury drop electrode (HMDE) with a drop area of 0.4 mm² was the working electrode. An Ag/AgCl/3M KCl electrode was the reference and a glassy carbon electrode was the auxiliary. Analysed samples were deoxygenated prior to measurement by purging with argon (99.999%). Acetate buffer (0.2 M CH₃COONa + CH₃COOH, pH 5), which was exchanged after each analysis, was used as a supporting electrolyte. The parameters of the measurement were as follows: initial potential of −1.3 V, end potential −0.6 V, deoxygenating with argon 90 s, accumulation time 240 s, time interval 0.04 s, step potential 5 mV, modulation amplitude 25 mV, deposition potential −1.15 V, volume of injected sample: 20 µL, volume of measurement cell 2,000 µL (20 µL of sample + 1,980 µL acetate buffer).

2.5. Atomic Absorption Spectrometry (AAS)

Determination of zinc was carried out on a 240FS atomic absorption spectrometer (Agilent Technologies, Santa Clara, CA, USA) equipped with flame atomization. The zinc hollow cathode lamp

(Agilent) operated at the current of 5 mA. Zinc was measured on the primary wavelength of 213.9 nm with a spectral bandwidth of 1.0 nm. A mixture of air and acetylene was used to atomize the zinc in the flame. Deuterium correction of background was used and the signal was measured in an integration mode for 2 s.

2.6. Amino Acid Analysis (AAA)

An AAA 400 liquid chromatography apparatus (Ingos, Prague, Czech Republic) was used to determine the amino acid histidine. The system consisted of a glassy filling chromatographic column and a steel precolumn, two chromatographic pumps for transportation of elution buffers and derivatization reagent, a cooled carousel for 25 test tubes of 1.5–2.0 mL volume, a dosing valve, a heat reactor, a visible detector and a cooled chamber for the derivatization reagent. The glassy chromatographic column (i.d. 3.7 mm and 350 mm length) was filled with LG ANB strong catex in sodium cycle (Spolchemie, Usti nad Labem, Czech Republic) with particles of an average size of 12 μm and a netting of 8%. The glassy column was tempered by a thermostat working in the interval from 35 to 95 $^{\circ}\text{C}$ range. The precolumn was filled with LG KS0804 ionex (Ingos). Chromatographic columns are able to work at a flow rate 0.01–10 mL/min under a maximum pressure of 40 MPa. Volume of injected sample was 100 μL with an accuracy of application RSD of about 1%. A two-channel VIS detector with a 5 μL flow volume cuvette was operated at wavelengths of 440 and 570 nm. Ninhydrin solution (Ingos) was used as a derivatization reagent. Ninhydrin was dissolved in a solution containing 75% (v/v) of the organic solvent methyl cellosolve (Ingos) and 25% (v/v) of 4 M acetate buffer (pH 5.5). SnCl_2 (Lachema, Brno, Czech Republic) was used as a reducing agent. Derivatization reagent was stored for the whole time under an inert atmosphere (N_2) with cooling at 4 $^{\circ}\text{C}$. During the analysis, the flow rate of mobile phase was set at 0.3 mL/min under a pressure ranging from 4.5 to 6.0 MPa. Reactor temperature was set to 120 $^{\circ}\text{C}$.

2.7. Electrospray Ionization Quadrupole Time-of-Flight (ESI-QTOF) Mass Spectrometer

Samples was prepared in acetonitrile (MS purity) with a 1% addition of formic acid and characterized by a Bruker Maxis Impact Q-TOF mass spectrometer (Bruker, Billerica, MA, USA). ESI source was operated in the positive mode. Voltage of an electrospray capillary was set to 3,500 V with a flow rate of nebulizing gas of 4 L/min and a drying gas temperature was set to 350 $^{\circ}\text{C}$. Flow rate of samples was set up to 180 $\mu\text{L}/\text{h}$.

2.8. Scanning Electron Microscopy (SEM) Characterisation of Modified Dowexmicroparticles

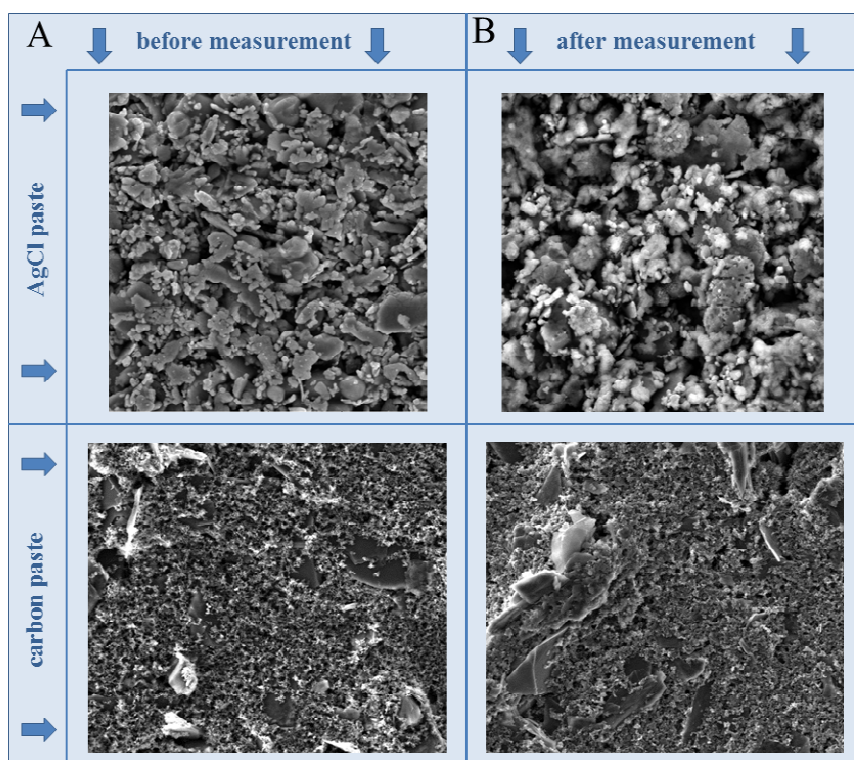
Structural and elemental composition of the screen-printed sensor were characterised by an electron microscope. For documentation of the selected nanomaterials, a FEG-SEM MIRA XMU instrument (Tescan, a.s., Brno, Czech Republic) was used. This model is equipped with a high brightness Schottky field emitter for low noise imaging at fast scanning rates. The SEM was fitted with Everhart-Thronley type of SE detector, a high speed YAG scintillator based BSE detector, a panchromatic CL Detector and EDX spectrometer. The MIRA 3 XMU system is based on a large specimen chamber with motorized stage movements of 130 \times 130 mm. Samples were coated by 10 nm of carbon to prevent

charging. A carbon coater K950X (Quorum Technologies, Grinstead, UK) was used. For automated acquisition of selected areas, a TESCAN proprietary software tool called Image Snapper was used. The software enables automatic acquisition of selected areas with defined resolution. Different conditions were used in order to obtain either minimum analysis time or maximum detail during overnight automated analysis. An accelerating voltage of 15 kV and beam currents of about 1 nA gave satisfactory results regarding maximum throughput.

3. Results and Discussion

In this study, we focused on the electrochemical analysis of four zinc compounds using a microfluidic system that consisted of a flow cell for printed sensors (electrodes). The surface of the printed electrodes, consisting of carbon and silver chloride (AgCl) paste, was characterized using SEM (Figure 1). It clearly follows from the results obtained that the surface of the working electrode did not change during the measurement, however, the surface of the reference one was slightly changed. This is given by chloride included in the paste which is little bit dissolved into the solution during the measurement. This could be associated with the fact that the electrochemical reaction monitored on the surface of the working electrode influenced the reference one. This is one of the reasons of the disposability of the printed electrodes. The great advantage of carbon paste is its ability to be modified easily by various agents (nanoparticles) to achieve better sensitivity and selectivity [39–42].

Figure 1. SEM photos of AgCl and carbon electrodes of SPE before and after measurement.

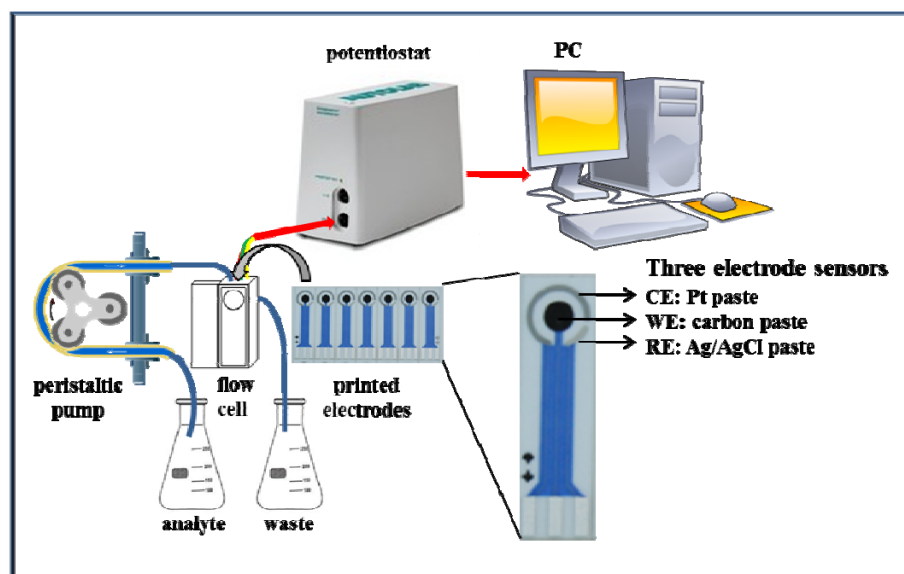


In recent years, a growing interest in fast, reliable and inexpensive sensors to determine the different types of analytes in biomedical, environmental and industrial samples has been shown [43–45]. The

method described in the Section 2.3 (*Three electrode system*) was chosen because of easy instrumentation (easy to use) and a possibility of setting variable flows [46].

The functionality of the suggested microfluidic system with electrochemical detection was tested firstly on zinc nitrate. The microfluidic system consisted of a workstation (PC), a potentiostat, a peristaltic pump and a flow cell for printed electrodes (Figure 2). The great advantage of this system is easy operation and service, thus, such systems can be used in a wide range of applications [47–49].

Figure 2. Schematic diagram of the microfluidic system with electrochemical detection.



During electrochemical analysis of 20 μM zinc nitrate reduction the zinc signals were monitored [50] under strictly defined conditions (pH, temperature, flow rate, time accumulation, applied potential) and are shown in Figure 3A. Firstly, we monitored the dependence of the reduction signal of Zn(II) ions on the change in pH value. Acetate buffers (pH 3.5, 4, 4.5, 5 and 5.5) were used for all electrochemical analyses. Application of 0.2 M acetate buffer, pH = 4.5, led to a twofold increase of intensity of the signal (Figure 3B). Temperature (10–50 $^{\circ}\text{C}$), potential (from -0.6 to -1.4 V), flow rate (from 0 to 1,280 $\mu\text{L}/\text{min}$), and time of accumulation (from 5 to 140 s) were other tested parameters. The best response (signal intensity) of the Zn(II) reduction signal was achieved at 40 $^{\circ}\text{C}$ (Figure 3C), applied potential -1.2 V (Figure 3D), flow rate 1,280 $\mu\text{L}/\text{min}$, where the most significant changes were evident up to the flow rate 133.5 $\mu\text{L}/\text{min}$ (Figure 3E), and accumulation time 90 s (Figure 3F). With increasing time of accumulation signal intensity first increased (up to 90 s) and then slightly decreased (90–120 s, Figure 3F). The potential was significantly shifted to more positive values with the increasing time of accumulation.

Calibration curve of Zn(II) ions using differential pulse voltammetry (DPV) is shown in Figure 3G. The dependence of concentration on the change in electrochemical signal was exponential with a coefficient of determination $R^2 = 0.9909$ (Figure 3G). To compare our electrochemical results, we also utilized standard hanging mercury drop electrode (HMDE) for determination of zinc(II) ions. The measured dependence of concentration on the change of signal was linear with a coefficient of determination $R^2 = 0.9927$ and is shown in Figure 3H. It clearly follows from the results that the results obtained using SPE are comparable to those obtained by HMDE. Zinc nitrate was further

characterized by UV/VIS spectrophotometry. The absorption spectrum was monitored within the range from 230 to 350 nm. In this range, no absorption maxima were detected, and the signal was only slightly increased at $\lambda = 230$ nm (Figure 3I). 2-(5-Bromo-2-pyridylazo)-5-[N-propyl-N-(3-sulfopropyl) amino]phenol disodium salt dehydrate (5-brom-PAPS) was used to detect Zn. This compound creates a coloured product with Zn(II) that can be detected at $\lambda = 550$ nm [51]. The spectrophotometric record of the product with absorption maximum is shown in Figure 3J. In the next step, we characterized electrochemical behaviour of two zinc complexes, (Zn(phen)(his)Cl₂ and Zn(his)Cl₂), and zinc-based nanoparticles (ZnS QDs).

Figure 3. Electrochemical and spectrophotometric analysis of Zn(NO₃)₂. Basic parameters were 20 μ M Zn(NO₃)₂ in 0.2 M acetate buffer, pH 5, temperature 20 °C unless stated otherwise. Electrochemical analysis of the Zn (II) ions using DPV (A) DP voltammogram of zinc nitrate. The effect of (B) pH (3.5–5.5), (C) temperature (10–50 °C), (D) applied potential (−1.4–−0.6 V), (E) applied flow rate (0–1,280 μ L/min), (F) time of accumulation (5–120 s), and (G) Calibration curve of Zn (II) ions using DPV, dependence of used concentration of zinc nitrate (0–125 μ M) on the change of reduction signal. (H) Dependence of used concentration of zinc nitrate on the change of reduction signal monitored using HMDE. In Figures B, C, and F, the blue columns represent height of signals (peaks, left scale), red squares indicate the potential at which the height of signals was detected (right scale). Spectrophotometric analysis of the Zn (II) ions. (I) Spectrophotometric record of the Zn(II) ions within the range from 230 to 380 nm. (J) Spectrophotometric record of the coloured product of the reaction of Zn(NO₃)₂ with 5-brom-PAPS with absorption maximum at $\lambda = 550$ nm.

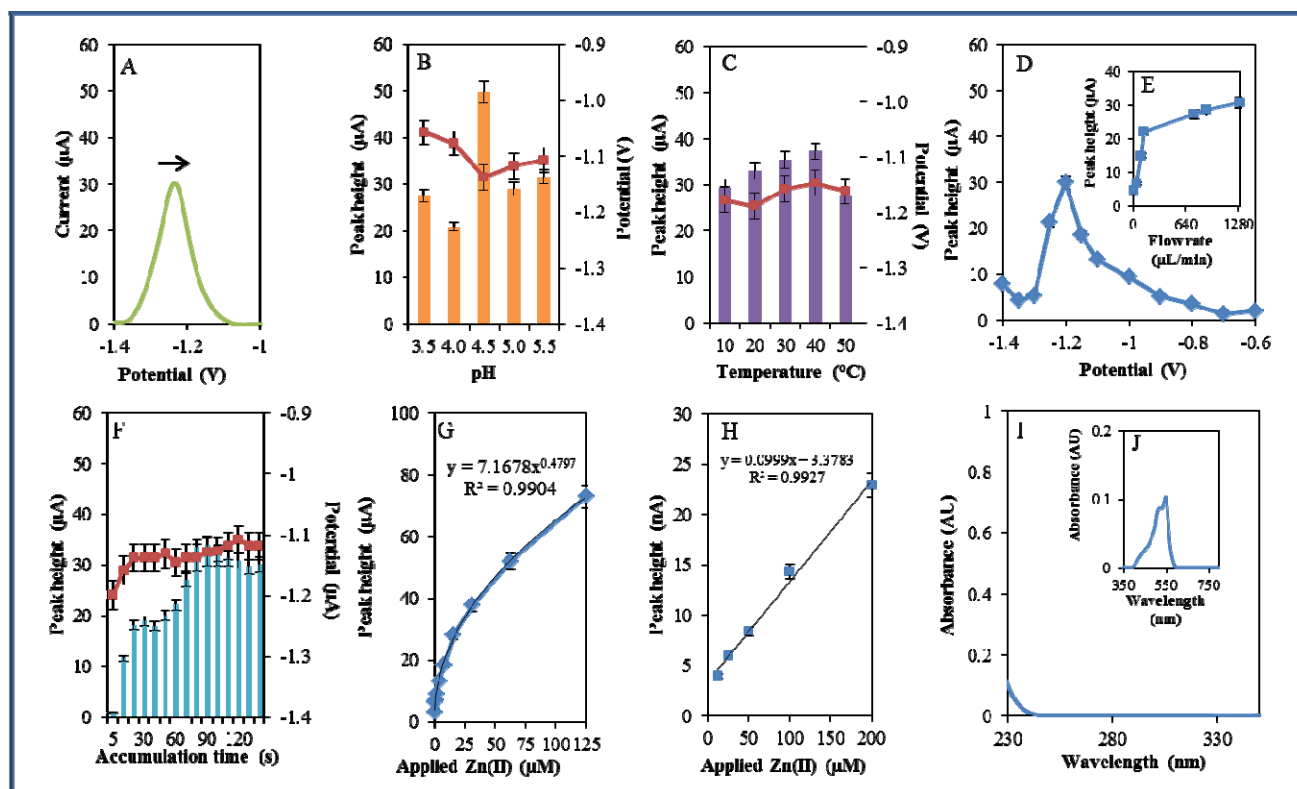
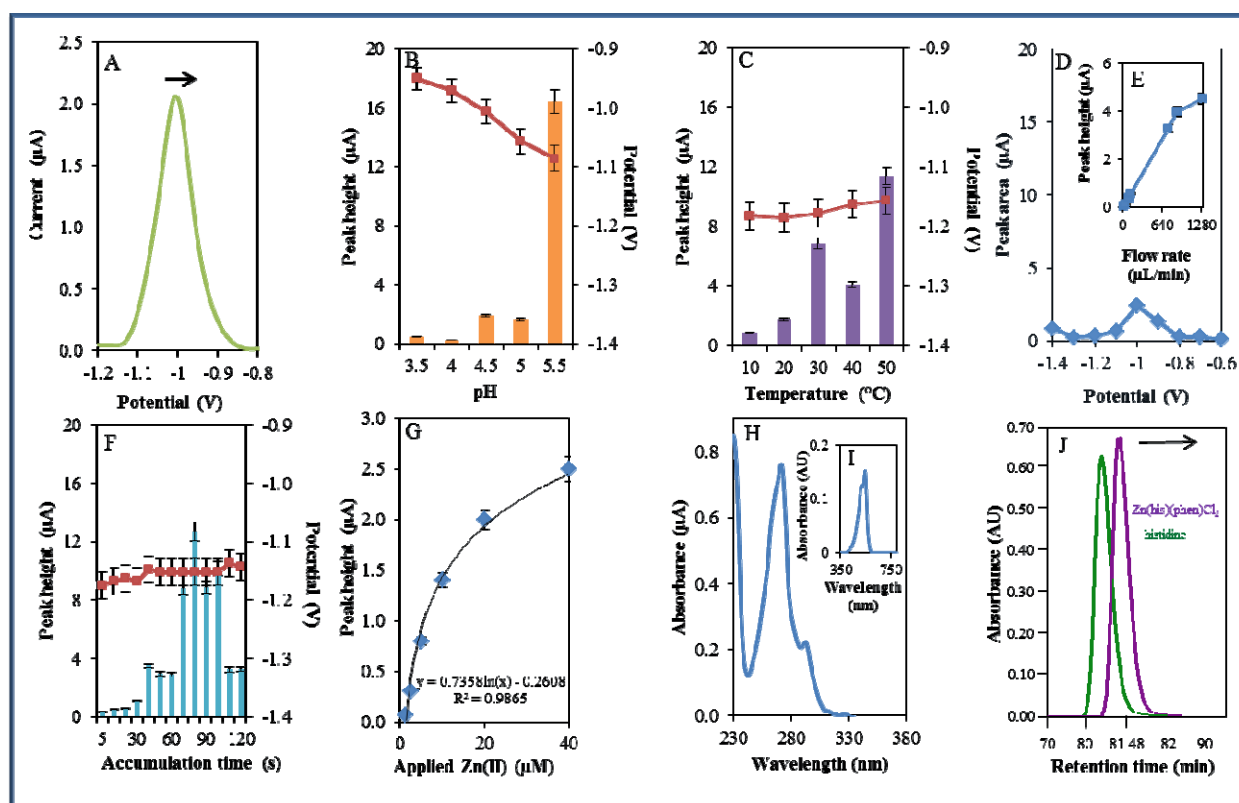


Figure 4. Electrochemical, spectrophotometric and chromatographic analysis of Zn(phen)(his)Cl₂ complex. Basic parameters were 20 μM Zn(phen)(his)Cl₂ in 0.2 M acetate buffer, pH 5, temperature 20 °C unless stated otherwise. Electrochemical analysis of the Zn(phen)(his)Cl₂ complex using DPV. **A**) DP voltammogram of Zn(phen)(his)Cl₂. Change in the height of reduction signal of Zn(phen)(his)Cl₂ influenced by **(B)** pH (3.5–5.5), **(C)** temperature (10–50 °C), **(D)** applied potential (−1.4–−0.6 V), **(E)** applied flow rate (0–1,280 μL/min), **(F)** time of accumulation (5–120 s), and **(G)** Calibration curve of Zn(II) ions using DPV, dependence of used concentration of Zn(II) ions in the complex (1–40 μM) on the change of reduction signal. In Figures **B**, **C**, and **F**, the blue columns represent height of signals (peaks, left scale), red squares indicate the potential at which the height of signals was detected (right scale). Spectrophotometric and chromatographic analysis of the Zn(phen)(his)Cl₂ complex. **(H)** Spectrophotometric record of Zn(phen)(his)Cl₂ measured within the range from 230 to 380 nm. **(I)** Detection of Zn(II) ions using spectrophotometric record of the colored product of the reaction of Zn(phen)(his)Cl₂ with 5-brom-PAPS with absorption maximum recorded at 550 nm. **(J)** Chromatogram demonstrating dependence of absorbance of histidine and Zn(phen)(his)Cl₂ on retention time.



3.1. Microfluidic Analysis with Electrochemical Detection of Zn(phen)(his)Cl₂ Complex

A microfluidic system with electrochemical detection was used to study the Zn(phen)(his)Cl₂ complex. In the experiment, we monitored the reduction signal of 20 μM Zn(phen)(his)Cl₂ (Figure 4A) under strictly defined experimental conditions as in the case of zinc nitrate. The highest signal was observed at pH 5.5. The recorded signal was on average eight times higher in comparison with lower

pH values (Figure 4B). The change from acidic (pH 3.5) to less acidic (pH 5.5) pH values was accompanied by a significant shift of the potential to more negative values. Bound Zn(II) in the complex is released by an increase in pH value. This fact has been confirmed in experiments with the changing pH (Figure 4B). A similar release of enclosed compounds depending on a change in pH value has been shown in the case of apoferritin [52,53] or in dual cargo delivery from mesoporous silica nanoparticles with a metal-latched nanogate [54].

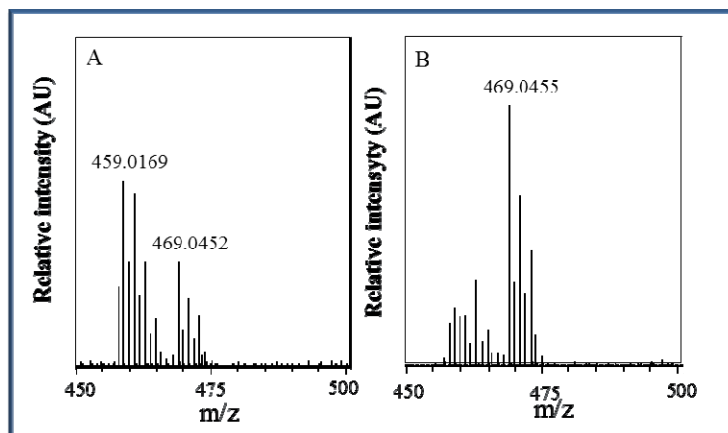
An increase in temperature (10–50 °C) had a contrary effect, and the signal was shifted to more positive values and the highest signal occurred at 50 °C at a potential of –1.15 V (Figure 4C). Changes in potential were further monitored amperometrically within the range from –1.4 to –0.6 V. The highest signal was recorded at a potential of –1 V (Figure 4D). The best response of the signal was well evident at the flow rate 640 µL/min (Figure 4E). The most suitable time of accumulation was established as 80 s. The potential showed a moderate shift to more positive values with the increasing time of accumulation (Figure 4F). Calibration curve of Zn(II) ions using DPV is shown in Figure 4G. The dependence of concentration on the change in electrochemical signal was logarithmic in concentration range 1–40 µM (Figure 4G)

The complex was further investigated by UV/VIS spectrophotometry. The absorption spectrum was monitored within the range from 230 to 350 nm. The complex showed two absorption maxima ($\lambda = 270$ and 291 nm, Figure 4H). Complex was further mixed with 2-(5-bromo-2-pyridylazo)-5-[N-propyl-N-(3-sulfopropyl)amino]phenol disodium salt dihydrate and incubated similarly as in the previous case. Formed colour product was identified at the same wavelength ($\lambda = 550$ nm) as zinc nitrate, which proved the presence of zinc [51]. Because the investigated complex contains the amino acid histidine, it was investigated using an automated amino acids analyser. L-Histidine (his) is an essential amino acid involved in the chelation of metal ions [55,56]. The chromatogram of the complex was compared with the chromatogram of a histidine standard. It was shown that signal of the standard occurred at a shorter retention time (80.67 min) than the signal of the complex (81.56 min). This fact indicates creation of the complex (Figure 4J).

3.2. Characterization of Zn(phen)(his)Cl₂ by ESI-QTOF Mass Spectrometry

Due to the behaviour of the zinc complex under various pH conditions and the non-linear calibration dependence, we attempted to analyse this complex using mass spectrometry. The ESI+ mass spectra display an intense signal at $m/z = 469$ that corresponds to the molecular ion Zn(his)(phen)Cl₂H⁺ and a signal at $m/z = 459$ that corresponds to the molecular ion Zn(his)(phen)(ACN)(H₂O)H⁺ with solvent molecules coordinating to the zinc central ion replacing coordinated chlorine ions. The height (intensity) of these peaks is closely connected with changes in pH value, as it can be seen in Figure 5A,B, respectively. At pH 5.5, the Zn(his)(phen)Cl₂ complex is more stable than at pH 3.5 and coordination of chlorine ions is preferred. In the spectra, there are also signals with lower $m/z = 383$, 367, and 314 that correspond to different complex fragments. All m/z interpretations are based on ³⁵Cl and ⁶⁴Zn, respectively.

Figure 5. ESI-QTOF mass spectrum of 10 μM $\text{Zn}(\text{phen})(\text{his})\text{Cl}_2$ measured within the range from 450 to 500 m/z in 0.2 M in the presence of acetate buffer (A) pH 3.5 and (B) pH 5.5.

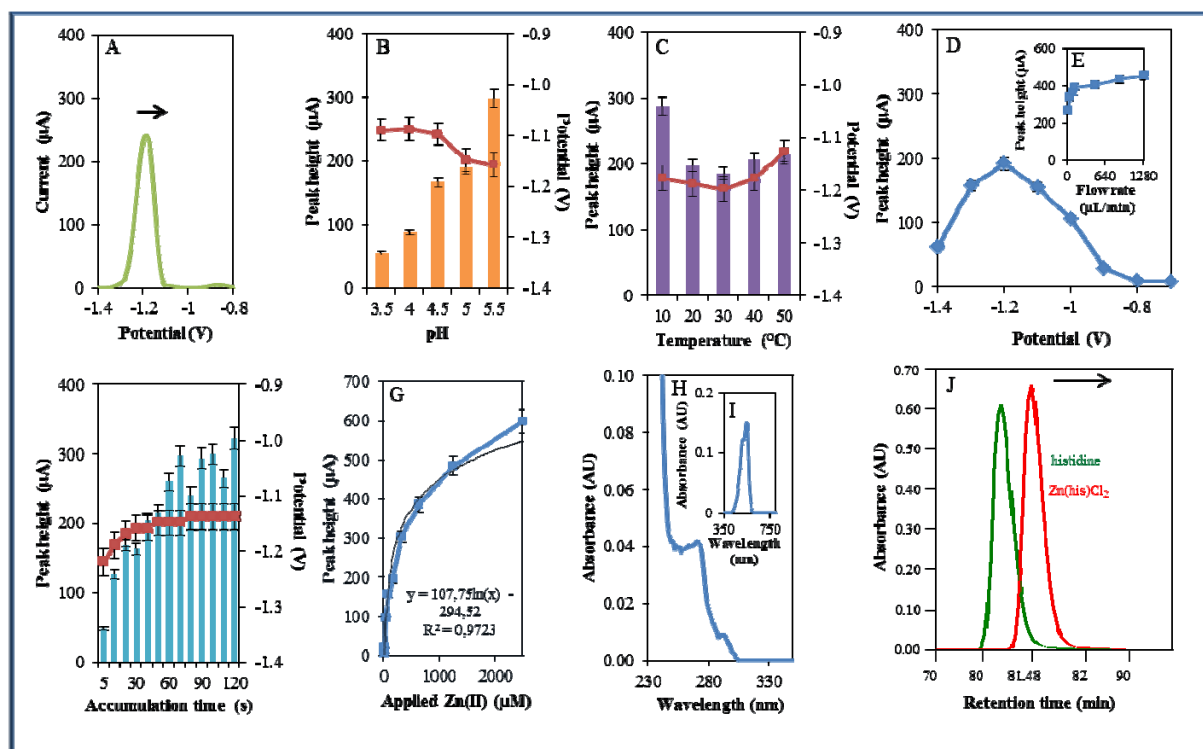


3.3. Microfluidic Analysis with Electrochemical Detection of $\text{Zn}(\text{his})\text{Cl}_2$ Complex

The other studied zinc complex did not contain a phenanthroline nitrogen-containing ligand, but only the amino acid histidine. Metal complexes of histidine may exhibit catalytic activity, especially with molybdenum, in oxidation reactions, as was shown by Vassilev *et al.* [55]. Due to the catalytic properties of Zn-his complexes, their possible application as catalysts was investigated [56]. In this study, $\text{Zn}(\text{his})\text{Cl}_2$ was studied by the same way as $\text{Zn}(\text{phen})(\text{his})\text{Cl}_2$ (Figure 6A). The highest signal was determined using 0.2 M acetate buffer of pH 5.5. This signal was six times higher compared to that measured in the presence of 0.2 M acetate buffer pH 3.5. The movement from (pH 3.5) to less acidic (pH 5.5) pH was accompanied by the shift of the potential to more negative values (Figure 6B) as in the case of $\text{Zn}(\text{phen})(\text{his})\text{Cl}_2$.

The increasing temperature (20–50 $^{\circ}\text{C}$) had almost no effect on the signal height. Higher temperature (30–50 $^{\circ}\text{C}$) led to a signal shift to more positive values. Temperature of 10 $^{\circ}\text{C}$ and applied potential -1.18 were determined as the most advantageous (Figure 6C). Changes in potential were further monitored amperometrically within the range from -1.4 to -0.6 V. The highest signal was observed at potential -1.2 V (Figure 6D) similarly to that observed for zinc nitrate. Optimal signal was determined at the flow rate 320 $\mu\text{L}/\text{min}$ (Figure 6E). The most suitable time of accumulation was determined as 120 s, where the potential showed a shift to more positive values with increasing time (potential shifted in the range of the time of accumulation 5–30 s, after that it was constant, Figure 6F). Calibration curve of Zn(II) ions using DPV is shown in Figure 6G. The dependence of concentration on the change in electrochemical signal was logarithmic with a coefficient of determination $R^2 = 0.9723$ (Figure 6G). $\text{Zn}(\text{his})\text{Cl}_2$ was finally characterized by UV/VIS spectrophotometry. The absorption maximum was recorded at $\lambda = 270$ nm. Presence of Zn(II) in 500 μM $\text{Zn}(\text{his})\text{Cl}_2$ was proved spectrophotometrically by the colour reaction recorded at $\lambda = 550$ nm [51]. Complex was also investigated by automated analyser of amino acids by the same way as $\text{Zn}(\text{phen})(\text{his})\text{Cl}_2$. Signal of the standard occurred at a shorter retention time (80.67 min) compared to that of studied complex (81.18 min). This fact verified creation of complex (Figure 6J). Studied complex ($\text{Zn}(\text{his})\text{Cl}_2$) eluted 0.38 min earlier than that of $\text{Zn}(\text{phen})(\text{his})\text{Cl}_2$. This result verified differences between these two studied complexes.

Figure 6. Electrochemical, spectrophotometric and chromatographic analysis of Zn(his)Cl₂ complex. Basic parameters were 200 μM Zn(phen)(his)Cl₂ in 0.2 M acetate buffer, pH 5, temperature 20 °C unless stated otherwise. Electrochemical analysis of the Zn(his)Cl₂ complex using differential pulse voltammetry (DPV). (A) DP Zn(his)Cl₂ voltammogram. The effect of (B) pH (3.5–5.5), (C) temperature (10–50 °C), (D) applied potential (−1.4–−0.6 V), (E) applied flow rate (0–1,280 μL/min), (F) time of accumulation (5–120 s), and (G) Calibration curve of Zn (II) ions using DPV, dependence of used concentration of Zn(II) ions in the complex (1–2,500 μM) on the change of reduction signal. In Figures B, C, and F, the blue columns represent height of signals (peaks, left scale), red squares indicate the potential at which the height of signals was detected (right scale). Spectrophotometric and chromatographic analysis of the Zn(his)Cl₂ complex. (H) Spectrophotometric record of complex measured within the range from 230 to 380 nm. (I) Detection of Zn(II) ions using spectrophotometric record of the colored product of the reaction of Zn(his)Cl₂ with 5-brom-PAPS with absorption maximum recorded at 550 nm. (J) Chromatogram demonstrating dependence of absorbance of histidine and Zn(his)Cl₂ complex on retention time.

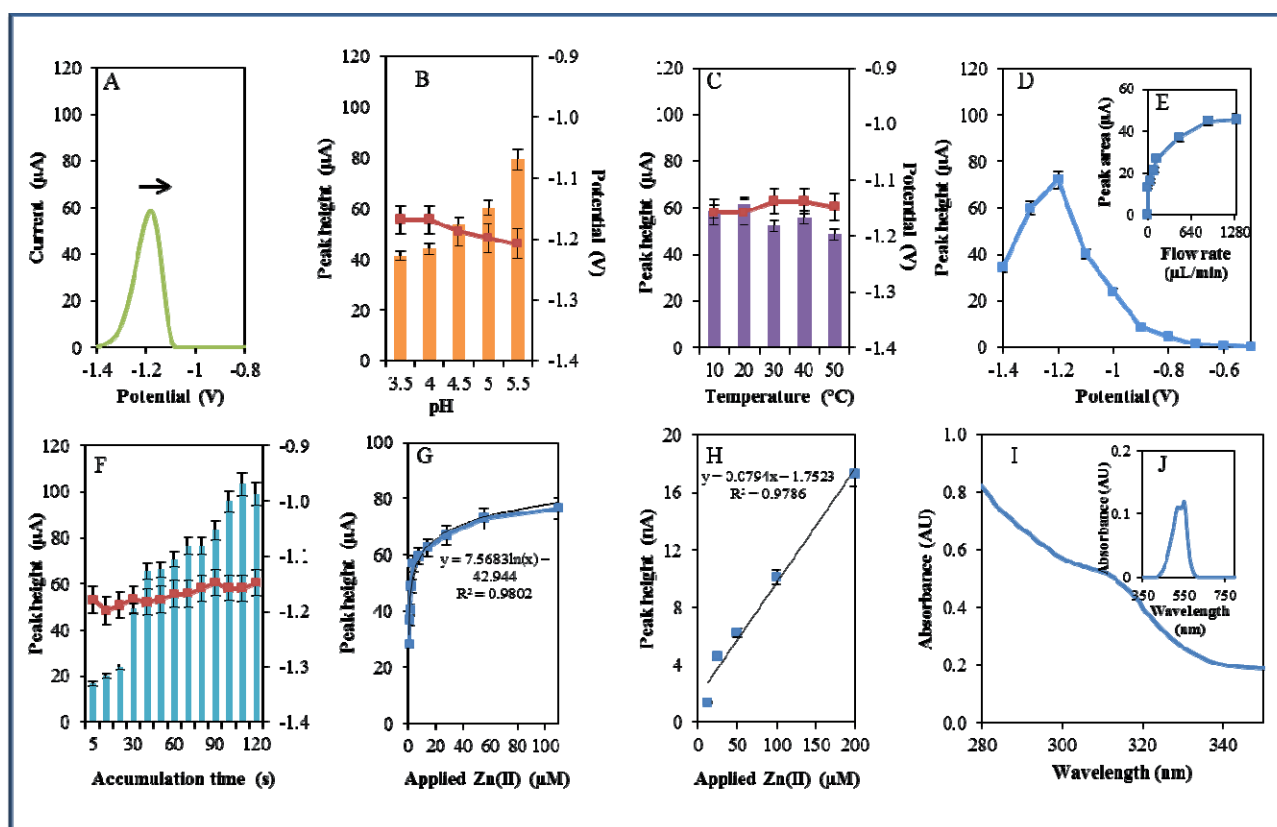


3.4. Flow Analysis of ZnS QDs

Quantum dots (QDs) are fluorescent semiconductor nanocrystals in the size ranging from 1 to 20 nm. They have specific optical and electronic properties depending on the ratio of the surface area to volume and on the so-called “quantum confinement” phenomenon. As a developing semiconductor material star, ZnS nanoparticles (NPs) are material with low toxicity [57] and with a wide band gap [14]. They exhibit remarkable optical and electrical properties [58–60], which suggest that they may be particularly well-suited for manufacturing novel sensors [61,62]. ZnS quantum dots were

studied by the use of microfluidic electrochemical analysis. Identically as in the previous compounds studied, the reduction potential of zinc in 20 μM ZnS QD was analysed (Figure 7A). The highest signal was observed under the use of 0.2 M acetate buffer at pH 5.5. The recorded signal increased on average by 11% with decreasing pH value (by 0.5 pH units) of the used buffer.

Figure 7. Electrochemical and spectrophotometric analysis of ZnS QDs. Basic parameters were 20 μM ZnS QDs in 0.2 M acetate buffer, pH 5, temperature 20 $^{\circ}\text{C}$ unless stated otherwise. Electrochemical analysis of the ZnS QDs using differential pulse voltammetry (DPV). (A) DP voltammogram of ZnS QDs. The effect of (B) pH (3.5–5.5; 0.2 M acetate buffer), (C) temperature (10–50 $^{\circ}\text{C}$), (D) applied potential (−1.4–−0.6 V), (E) applied flow rate (0–1,280 $\mu\text{L}/\text{min}$), (F) time of accumulation (5–120 s), and (G) Calibration curve of Zn(II) ions using DPV, dependence of used concentration of Zn(II) ions in ZnS QDs (1–110 μM) on the change of reduction signal. (H) Dependence of applied concentration of ZnS QDs on the change of signal recorded using HMDE. In Figures B, C, and F, the blue columns represent height of signals (peaks, left scale), red squares indicate the potential at which the height of signals was detected (right scale). Spectrophotometric analysis of the ZnS QDs. (I) Spectrophotometric record of ZnS QDs within the range from 230 to 380 nm. (J) Detection of Zn(II) ions using spectrophotometric record of the coloured product of the reaction of ZnS QDs with 5-brom-PAPS with absorption maximum recorded at 550 nm.



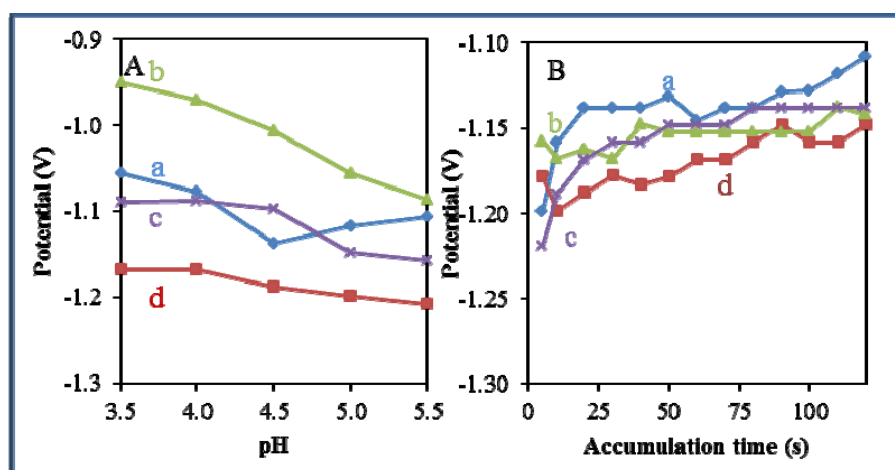
The movement from acidic (pH 3.5) to less acidic pH (pH 5.5) was accompanied by a significant shift of the potential to more negative values (Figure 7B) in the same way as that seen in Zn(phen)(his)Cl₂ and Zn(his)Cl₂. The increasing temperature (10–50 $^{\circ}\text{C}$) led to the change in the

height of signal and has almost no effect on the signal shift. The best results were recorded at a temperature of 20 °C, and -1.16 V applied potential (Figure 7C). Changes in potential were further investigated amperometrically within the range from -1.4 to -0.6 V. Applied potential of -1.2 V showed the highest signal (Figure 7D). The same results were observed in the case of zinc nitrate and Zn(his)Cl₂ complex. Height of the signal increased up to the flow rate of 892 $\mu\text{L}/\text{mL}$, after that the recorded signal remained unchanged (Figure 7E). The most suitable time of accumulation was determined as 110 s, where the potential showed a moderate shift to more positive values with the increasing time of accumulation (Figure 7F). Calibration curve of Zn(II) ions using DPV is shown in Figure 7G. Dependence of concentration on the change in electrochemical signal was logarithmic, with the coefficient of determination $R^2 = 0.9802$ (Figure 7G). Reduction signals of Zn(II) were also investigated by the use of HMDE. The dependence of concentration on the change in signal was linear with a coefficient of determination $R^2 = 0.9786$ (Figure 7H). ZnS QDs were finally characterized by UV/VIS spectrophotometry the same way as the complexes and zinc nitrate studied previously. A moderate increase in absorbance at 313 nm was detected (Figure 7I). The presence of Zn(II) in 20 μM ZnS QD was proved spectrophotometrically in the same way as the complexes studied previously (Figure 7J).

3.5. Comparison of Effect of pH and Time of Accumulation on the Change in Potential

A significant effect of pH and time of accumulation on the change in potential was observed in all studied zinc-based compounds and quantum dots. Changes in pH led to a shift of the electrochemical signal to more negative values (Figure 8A). The most significant effect of pH was recorded for Zn(phen)(his)Cl₂ (Figure 8A-b). On the other hand, an adverse effect was observed in the case of the time of accumulation, where potential shifted from negative to more positive values with the increasing time of accumulation (Figure 8B). The most significant effect of the time of accumulation on the change in potential was recorded for zinc nitrate (Figure 8B-a) and Zn(his)Cl₂, (Figure 8B-c).

Figure 8. Dependence of height of signal on the change in pH value (3.5–5.5) and time of accumulation (5–120 s) of studied zinc-based compounds as (A) (a = zinc nitrate, b = Zn(phen)(his)Cl₂, c = Zn(his)Cl₂, and d = ZnS-QD), and (B) (a = zinc nitrate, b = Zn(phen)(his)Cl₂, c = Zn(his)Cl₂, and d = ZnS-QD).



3.6. Summary of the Characterization Results

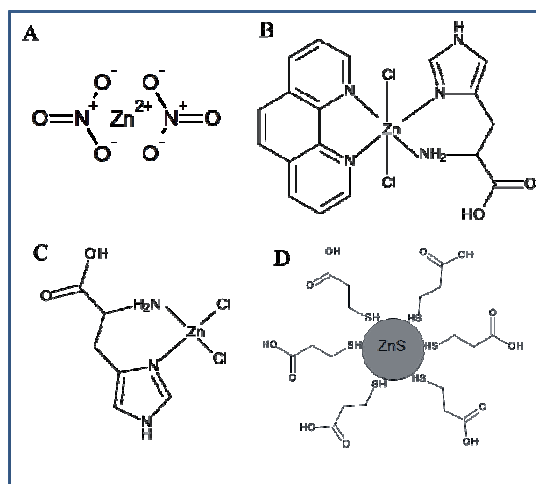
Table 1 summarizes the optimal conditions for the electrochemical study of zinc complexes and ZnS QDs using microfluidic analysis. Investigated zinc compounds were studied at a potential of -1.2 V, with the exception of Zn(phen)(his)Cl₂, which showed an electrochemical signal at the potential of -1 V. The most suitable conditions for the study of complexes were achieved using 0.2 M acetate buffer pH 5.5 with the exception of zinc nitrate, which was well detected in the same buffer, but at pH 4.5. The largest differences were observed in the temperature optimization of the detection of zinc complexes. The complex Zn(his)Cl₂ showed the strongest electrochemical signal at 10 °C, whereas at the complex Zn(phen)(his)Cl₂ the strongest signal was achieved at 50 °C. The optimal temperature for the electrochemical analysis of zinc nitrate was 40 °C and for the analysis of ZnS QD it was 20 °C. For all investigated samples it was observed that with higher flow the electrochemical signal was also increasing. The highest signals were obtained under the flow rate 1,300 μ L/min. Due to the saving of samples the optimal flow rate was always chosen. The lowest flow rate was set for nitrate (135.5 μ L/min), while the highest was for ZnS QDs (892 μ L/min). For Zn(phen)(his)Cl₂ and Zn(his)Cl₂ the same flow rate (320 μ L/min) was used. The longest accumulation time (100 s) was set for Zn(his)Cl₂ and ZnS QD. The shortest accumulation time (80 s) was chosen for Zn(phen)(his)Cl₂ and zinc nitrate (90 s).

Table 1. Summary table with the optimal conditions for microfluidic analysis.

	Potential (V)	pH	Temperature (°C)	Flow Rate (μ L/min)	Accumulation Time (s)
Zinc nitrate	-1.2	4.5	40	133.5	90
Zn(phen)(his)Cl ₂	-1	5.5	50	640	80
Zn(his)Cl ₂	-1.2	5.5	10	320	120
ZnS QD	-1.2	5.5	20	892	110

The whole work deals with the electrochemical study of zinc nitrate, zinc complexes and ZnS nanoparticles using a microfluidic flow system. The advantage of this system compared to HMDE is the possibility to miniaturize the entire system, which offers possibilities for other applications. The usability of HMDE is limited due to the high toxicity of mercury and small anodic range (limited by the oxidation of mercury). Another advantage of the applied method is the easy adjustability of different flow rates in order to achieve better electrochemical signals. When using HMDE these possibilities are not applicable. Printed electrodes can be modified by various substances in order to achieve better results in electrochemical analysis, but the options of HMDE in this respect are very limited. Flow systems containing printed electrodes are generally easier to use. HMDE method is more demanding on the instrumentation owing to the fact that falling of mercury drops may occur. Printed electrodes in combination with a microfluidic flow system can be an alternative to electrochemical methods using HMDE. The results presented in this study should serve as a basis for further investigation of zinc compounds. Based on the results obtained in this study we suggested the structure of all compounds of interest (Figure 9).

Figure 9. Structure of (A) Zinc nitrate and suggested structure of zinc complexes as (B) Zn(phen)(his)Cl₂, (C) Zn(his)Cl₂ and (D) ZnS QDs covered with 3-mercaptopropionic acid.



4. Conclusions

This study presents an electrochemical study of four zinc-based compounds by the use of flow cells and printed electrodes. The method was first optimized using zinc nitrate. We then monitored the electrochemical reduction signals of Zn(phen)(his)Cl₂, Zn(his)Cl₂, and ZnS QD nanoparticles. Complexes were further characterized by UV/VIS spectrophotometry, chromatography, and ESI-QTOF mass spectrometry. Complexes of zinc with 1,10-phenanthroline which is a universal chelating agent were described and the use of zinc nanoparticles has been growing [5,63–66]. Investigating these complexes is urgently required due to their biological activity. They are able to bind and cleave DNA. In addition, they present significant antimicrobial activity.

Acknowledgments

Financial support from the projects PGS15 2012 and CEITEC CZ.1.05/1.1.00/02.0068 is highly acknowledged.

Conflicts of Interest

The authors declare no conflict of interest.

References

1. Cummings, J.E.; Kovacic, J.P. The ubiquitous role of zinc in health and disease. *J. Vet. Emerg. Crit. Care* **2009**, *19*, 215–240.
2. Falchuk, K.H. The molecular basis for the role of Zinc in developmental biology. *Mol. Cell. Biochem.* **1998**, *188*, 41–48.
3. Klug, A. The discovery of Zinc fingers and their development for practical applications in gene regulation and genome manipulation. *Q. Rev. Biophys.* **2010**, *43*, 1–21.

4. Zalewski, P.D.; Millard, S.H.; Forbes, I.J.; Kapaniris, O.; Slavotinek, A.; Betts, W.H.; Ward, A.D.; Lincoln, S.F.; Mahadevan, I. Video image-analysis of labile Zinc in viable pancreatic-islet cells using a specific fluorescent-probe for Zinc. *J. Histochem. Cytochem.* **1994**, *42*, 877–884.
5. Fujimoto, S.; Yasui, H.; Yoshikawa, Y. Development of a novel antidiabetic Zinc complex with an organoselenium ligand at the lowest dosage in KK-A(y) mice. *J. Inorg. Biochem.* **2013**, *121*, 10–15.
6. Hosek, J.; Novotna, R.; Babula, P.; Vanco, J.; Travnicek, Z. Zn(II)-Chlorido complexes of phytohormone kinetin and its derivatives modulate expression of inflammatory mediators in THP-1 cells. *PLoS One* **2013**, *8*, 1–9.
7. Wu, S.P.; Du, Y.M.; Hu, Y.Z.; Shi, X.W.; Zhang, L.N. Antioxidant and antimicrobial activity of xylan-chitooligomer-zinc complex. *Food Chem.* **2013**, *138*, 1312–1319.
8. Chifotides, H.T.; Dunbar, K.R. Interactions of metal-metal-bonded antitumor active complexes with DNA fragments and DNA. *Account Chem. Res.* **2005**, *38*, 146–156.
9. Tapiero, H.; Tew, K.D. Trace elements in human physiology and pathology: Zinc and metallothioneins. *Biomed. Pharmacother.* **2003**, *57*, 399–411.
10. Reddy, P.R.; Manjula, P. Mixed-Ligand copper(II)-phenanthroline-dipeptide complexes: Synthesis, characterization, and DNA-cleavage properties. *Chem. Biodivers.* **2007**, *4*, 468–480.
11. Reddy, P.R.; Raju, N. Synthesis and characterization of novel square planar copper(II)-dipeptide-1,10-phenanthroline complexes: Investigation of their DNA binding and cleavage properties. *Polyhedron* **2012**, *44*, 1–10.
12. Tabassum, S.; Asim, A.; Arjmand, F.; Afzal, M.; Bagchi, V. Synthesis and characterization of copper(II) and zinc(II)-based potential chemotherapeutic compounds: Their biological evaluation viz. DNA binding profile, cleavage and antimicrobial activity. *Eur. J. Med. Chem.* **2012**, *58*, 308–316.
13. Fang, X.S.; Wu, L.M.; Hu, L.F. ZnS nanostructure arrays: A developing material star. *Adv. Mater.* **2011**, *23*, 585–598.
14. Fang, X.S.; Zhai, T.Y.; Gautam, U.K.; Li, L.; Wu, L.M.; Yoshio, B.; Golberg, D. ZnS nanostructures: From synthesis to applications. *Prog. Mater. Sci.* **2011**, *56*, 175–287.
15. Li, Y.C.; Li, X.H.; Yang, C.H.; Li, Y.F. Ligand-Controlling synthesis and ordered assembly of ZnS nanorods and nanodots. *J. Phys. Chem. B* **2004**, *108*, 16002–16011.
16. Lin, S.L.; Pradhan, N.; Wang, Y.J.; Peng, X.G. High quality ZnSe and ZnS nanocrystals formed by activating Zinc carboxylate precursors. *NANO Lett.* **2004**, *4*, 2261–2264.
17. Pal, S.; Goswami, B.; Sarkar, P. Size-Dependent properties of hollow ZnS nanoclusters. *J. Phys. Chem. C* **2008**, *112*, 6307–6312.
18. Li, H.; Shih, W.Y.; Shih, W.H. Synthesis and characterization of aqueous carboxyl-capped CdS quantum dots for bioapplications. *Ind. Eng. Chem. Res.* **2007**, *46*, 2013–2019.
19. Krejcová, L.; Huska, D.; Hýnek, D.; Kopel, P.; Adam, V.; Hubálek, J.; Trnková, L.; Kizek, R. Using of paramagnetic microparticles and quantum dots for isolation and electrochemical detection of influenza viruses' specific nucleic acids. *Int. J. Electrochem. Sci.* **2013**, *8*, 689–702.
20. Li, J.; Guo, S.J.; Zhai, Y.M.; Wang, E.K. Nafion-Graphene nanocomposite film as enhanced sensing platform for ultrasensitive determination of cadmium. *Electrochem. Commun.* **2009**, *11*, 1085–1088.

21. Muntyanu, G.G. Electroanalytical properties of a thin-film mercury-carbon electrode of subnanometric thickness in high-speed linear-sweep anodic stripping voltammetry as exemplified by the determination of Zn(II), Cd(II), and Pb(II). *J. Anal. Chem.* **2004**, *59*, 760–767.
22. Jothimuthu, P.; Wilson, R.A.; Herren, J.; Pei, X.; Kang, W.; Daniels, R.; Wong, H.; Beyette, F.; Heineman, W.R.; Papautsky, I. Zinc detection in serum by anodic stripping voltammetry on microfabricated bismuth electrodes. *Electroanalysis* **2013**, *25*, 401–407.
23. Ramadan, A.A.; Mandil, H.; Hafez, B. Differential pulse polarographic determination of atorvastatin in pharmaceutical dosage forms using dropping mercury electrode. *Asian J. Chem.* **2013**, *25*, 3467–3472.
24. Souckova, J.; Skopalova, J.; Svecova, H.; Bartak, P. Fused-Silica capillary dropping mercury electrode for electrocapillary measurements. *Electroanalysis* **2013**, *25*, 174–178.
25. Nagles, E.; Arancibia, V.; Rios, R. Determination of lead and cadmium in the presence of Quercetin-5'-sulfonic acid by adsorptive stripping voltammetry with a hanging mercury drop electrode and a nafion-coated mercury film electrode. *Int. J. Electrochem. Sci.* **2012**, *7*, 4545–4558.
26. Sorger, P.K. Microfluidics closes in on point-of-care assays. *Nat. Biotechnol.* **2008**, *26*, 1345–1346.
27. Yager, P.; Edwards, T.; Fu, E.; Helton, K.; Nelson, K.; Tam, M.R.; Weigl, B.H. Microfluidic diagnostic technologies for global public health. *Nature* **2006**, *442*, 412–418.
28. Nugen, S.R.; Asiello, P.J.; Connelly, J.T.; Baeumner, A.J. PMMA biosensor for nucleic acids with integrated mixer and electrochemical detection. *Biosens. Bioelectron.* **2009**, *24*, 2428–2433.
29. Lei, K.F. Microfluidic systems for diagnostic applications: A review. *Jala* **2012**, *17*, 330–347.
30. Atalay, Y.T.; Vermeir, S.; Witters, D.; Vergauwe, N.; Verbruggen, B.; Verboven, P.; Nicolai, B.M.; Lammertyn, J. Microfluidic analytical systems for food analysis. *Trends Food Sci. Technol.* **2011**, *22*, 386–404.
31. Eicher, D.; Merten, C.A. Microfluidic devices for diagnostic applications. *Expert Rev. Mol. Diagn.* **2011**, *11*, 505–519.
32. Giridharan, V.; Yun, Y.; Hajdu, P.; Conforti, L.; Collins, B.; Jang, Y.; Sankar, J. Microfluidic Platforms for evaluation of nanobiomaterials: A review. *J. Nanomater.* **2012**, *2012*, 1–14.
33. Ricciardi, C.; Canavese, G.; Castagna, R.; Ferrante, I.; Ricci, A.; Marasso, S.L.; Napione, L.; Bussolino, F. Integration of microfluidic and cantilever technology for biosensing application in liquid environment. *Biosens. Bioelectron.* **2010**, *26*, 1565–1570.
34. Huang, Y.; Shi, M.; Zhao, S.L.; Liang, H. A sensitive and rapid immunoassay for quantification of testosterone by microchip electrophoresis with enhanced chemiluminescence detection. *Electrophoresis* **2011**, *32*, 3196–3200.
35. Weiss, V.U.; Bilek, G.; Pickl-Herk, A.; Blaas, D.; Kenndler, E. Mimicking virus attachment to host cells employing liposomes: Analysis by chip electrophoresis. *Electrophoresis* **2009**, *30*, 2123–2128.
36. Kumar, R.S.; Arunachalam, S. DNA binding and antimicrobial studies of polymer-copper(II) complexes containing 1,10-phenanthroline and L-phenylalanine ligands. *Eur. J. Med. Chem.* **2009**, *44*, 1878–1883.
37. Krejcova, L.; Dospivova, D.; Ryvolova, M.; Kopel, P.; Hynek, D.; Krizkova, S.; Hubalek, J.; Adam, V.; Kizek, R. Paramagnetic particles coupled with an automated flow injection analysis as a tool for influenza viral protein detection. *Electrophoresis* **2012**, *33*, 3195–3204.

38. Prasek, J.; Trnkova, L.; Gablech, I.; Businova, P.; Drbohlavova, J.; Chomoucka, J.; Adam, V.; Kizek, R.; Hubalek, J. Optimization of planar three-electrode systems for redox system detection. *Int. J. Electrochem. Sci.* **2012**, *7*, 1785–1801.
39. Arvand, M.; Vaziri, M.; Zanjanchi, M.A. Voltammetric characteristics of diazinon on carbon paste electrode modified with tris(ethylenediamine) cobalt(II) iodide. *J. Anal. Chem.* **2013**, *68*, 429–435.
40. Azizi, S.N.; Ranjbar, S.; Raouf, J.B.; Hamidi-Asl, E. Preparation of Ag/NaA zeolite modified carbon paste electrode as a DNA biosensor. *Sens. Actuator B-Chem.* **2013**, *181*, 319–325.
41. Aydogdu, G.; Zeybek, D.K.; Zeybek, B.; Pekyardimci, S. Electrochemical sensing of NADH on NiO nanoparticles-modified carbon paste electrode and fabrication of ethanol dehydrogenase-based biosensor. *J. Appl. Electrochem.* **2013**, *43*, 523–531.
42. Wang, Z.Q.; Liu, G.; Zhang, L.N.; Wang, H. A bismuth modified hybrid binder carbon paste electrode for electrochemical stripping detection of trace heavy metals in soil. *Int. J. Electrochem. Sci.* **2012**, *7*, 12326–12339.
43. Honeychurch, K.C.; Hart, J.P. Screen-Printed electrochemical sensors for monitoring metal pollutants. *TRAC-Trends Anal. Chem.* **2003**, *22*, 456–469.
44. Hart, J.P.; Crew, A.; Crouch, E.; Honeychurch, K.C.; Pemberton, R.M. Some recent designs and developments of screen-printed carbon electrochemical sensors/biosensors for biomedical, environmental, and industrial analyses. *Anal. Lett.* **2004**, *37*, 789–830.
45. Ashley, K. Developments in electrochemical sensors for occupational and environmental health applications. *J. Hazard. Mater.* **2003**, *102*, 1–12.
46. De Oliveira, P.R.; Oliveira, M.M.; Zarbin, A.J.G.; Marcolino, L.H.; Bergamini, M.F. Flow injection amperometric determination of isoniazid using a screen-printed carbon electrode modified with silver hexacyanoferrates nanoparticles. *Sens. Actuator B Chem.* **2012**, *171*, 795–802.
47. Alonso, G.A.; Dominguez, R.B.; Marty, J.L.; Munoz, R. An approach to an inhibition electronic tongue to detect on-line organophosphorus insecticides using a computer controlled multi-commuted flow system. *Sensors* **2011**, *11*, 3791–3802.
48. Trnkova, L.; Adam, V.; Hubalek, J.; Babula, P.; Kizek, R. Amperometric sensor for detection of chloride ions. *Sensors* **2008**, *8*, 5619–5636.
49. Jackson, W.C.; Leger, W.; Lopez, G.P.; Tran, H.D.; Rapid Prototyping of Microfluidic Components. In Proceedings of Annual Meeting American Society for Precision Engineering, Raleigh, NC, USA, 22–27 October 2000; pp. 588–591.
50. Altun, S.; Ozkaya, A.R.; Bulut, M. Peripheral octa-substituted metal-free, cobalt(II) and Zinc(II) phthalocyanines bearing coumarin and chloro groups: Synthesis, characterization, spectral and electrochemical properties. *Polyhedron* **2012**, *48*, 31–42.
51. Hayashibe, Y.; Takeya, M.; Sayama, Y. Direct determination of Zinc in human serum by flow-injection spectrophotometric analysis. *Anal. Sci.* **1994**, *10*, 795–799.
52. Kilic, M.A.; Ozlu, E.; Calis, S. A novel protein-based anticancer drug encapsulating nanosphere: Apoferritin-Doxorubicin complex. *J. Biomed. Nanotechnol.* **2012**, *8*, 508–514.
53. Dospivova, D.; Hynek, D.; Kopel, P.; Bezdekova, A.; Sochor, J.; Krizkova, S.; Adam, V.; Trnkova, L.; Hubalek, J.; Babula, P.; *et al.* Electrochemical behaviour of apoferritin encapsulating of Silver(I) Ions and its application for treatment of staphylococcus aureus. *Int. J. Electrochem. Sci.* **2012**, *7*, 6378–6395.

54. Tarn, D.; Xue, M.; Zink, J.I. pH-Responsive dual cargo delivery from mesoporous silica nanoparticles with a metal-latched nanogate. *Inorg. Chem.* **2013**, *52*, 2044–2049.
55. Vassilev, K.; Dimitrova, M.; Turmanova, S.; Milina, R. Catalytic activity of histidine-metal complexes in oxidation reactions. *Synth. React. Inorg. Met.-Org. Nano-Metal. Chem.* **2013**, *43*, 243–249.
56. Sahoo, P.C.; Jang, Y.N.; Lee, S.W. Immobilization of carbonic anhydrase and an artificial Zn(II) complex on a magnetic support for biomimetic carbon dioxide sequestration. *J. Mol. Catal. B-Enzym.* **2012**, *82*, 37–45.
57. Abbas, N.K.; Al-Rasoul, K.T.; Shanan, Z.J. New method of preparation ZnS Nano size at low pH. *Int. J. Electrochem. Sci.* **2013**, *8*, 3049–3056.
58. Dong, B.H.; Cao, L.X.; Su, G.; Liu, W.; Qu, H.; Zhai, H. Water-Soluble ZnS:Mn/ZnS core/shell nanoparticles prepared by a novel two-step method. *J. Alloy. Compd.* **2010**, *492*, 363–367.
59. Lu, C.L.; Gao, J.F.; Fu, Y.Q.; Du, Y.Y.; Shi, Y.L.; Su, Z.M. A ligand exchange route to highly luminescent surface-functionalized ZnS nanoparticles and their transparent polymer nanocomposites. *Adv. Funct. Mater.* **2008**, *18*, 3070–3079.
60. Wang, X.F.; Xu, J.J.; Chen, H.Y. A new electrochemiluminescence emission of Mn²⁺-Doped ZnS nanocrystals in aqueous solution. *J. Phys. Chem. C* **2008**, *112*, 17581–17585.
61. Mandal, A.; Dandapat, A.; De, G. Magic sized ZnS quantum dots as a highly sensitive and selective fluorescence sensor probe for Ag⁺ ions. *Analyst* **2012**, *137*, 765–772.
62. Patolsky, F.; Gill, R.; Weizmann, Y.; Mokari, T.; Banin, U.; Willner, I. Lighting-Up the dynamics of telomerization and DNA replication by CdSe-ZnS quantum dots. *J. Am. Chem. Soc.* **2003**, *125*, 13918–13919.
63. Qian, S.S.; Hu, X.; Liu, L.; You, Z.L.; Zhu, H.L. Synthesis and crystal structure of a tetranuclear Zinc(II) complex derived from 2-{ 1-(4-Diethylamino-2-hydroxy-phenyl)methylidene amino}-2-ethylpropane-1,3-diol. *Synth. React. Inorg. Met. Org. Nano-Metal. Chem.* **2013**, *43*, 847–851.
64. Lai, Q.Z.; Zhang, H.M.; Li, X.F.; Zhang, L.Q.; Cheng, Y.H. A novel single flow Zinc-bromine battery with improved energy density. *J. Power Sources* **2013**, *235*, 1–4.
65. Odabas, Z.; Orman, E.B.; Durmus, M.; Dumludag, F.; Ozkaya, A.R.; Bulut, M. Novel alpha-7-oxy-4-(4-methoxyphenyl)-8-methylcoumarin substituted metal-free, Co(II) and Zn(II) phthalocyanines: Photochemistry, photophysics, conductance and electrochemistry. *Dyes Pigment.* **2012**, *95*, 540–552.
66. Vazquez-Arenas, J.; Sosa-Rodriguez, F.; Lazaro, I.; Cruz, R. Thermodynamic and electrochemistry analysis of the Zinc electrodeposition in NH₄Cl-NH₃ electrolytes on Ti, Glassy Carbon and 316L Stainless Steel. *Electrochim. Acta* **2012**, *79*, 109–116.